JOURNAL OF COMPUTATIONAL PHYSICS 92, 230–256 (1991)

A Symplectic Integration Algorithm for Separable Hamiltonian Functions

J. CANDY AND W. ROZMUS

Department of Physics, University of Alberta, Edmonton, Alberta, Canada T6G 2J1

Received July 26, 1989; revised October 27, 1989

We derive an algorithm to numerically integrate differential equations derivable from a separable Hamiltonian function. This symplectic algorithm is accurate to fourth order in the time step and preserves exactly the Poincaré–Cartan integral invariants associated with the topology of the phase flow. We compare the efficiency and accuracy of this method to that of existing integrators (both symplectic and non-symplectic) by integrating the equations of motion corresponding to a nonlinear pendulum, a particle in the field of a standing wave, and a harmonic oscillator perturbed by a plane wave.

1. INTRODUCTION

The study of Hamiltonian dynamical systems leads quite often to differential equations which are not solvable analytically. Increasingly, numerical integration is being used to gain insight into the complicated behavior of such systems. Unfortunately, popular integration schemes—including the Runge–Kutta class of algorithms—do not take into account the Hamiltonian nature of the equations and, consequently, do not preserve the hierarchy of global invariants known to exist in these systems.

Consider, for example, a Hamiltonian system with N degrees of freedom and an N-dimensional configuration manifold $\mathscr{V}$. Let $\mathbf{q}$ be the local coordinates on $\mathscr{V}$. It can be shown that the cotangent bundle of $\mathscr{V}$, written $T^*\mathscr{V}$, has the structure of a $2N$-dimensional differentiable manifold with local coordinates $(\mathbf{q}, \mathbf{p})$, where $\mathbf{p}$ is the usual canonical momentum vector (see [1] for details). On the cotangent bundle $T^*\mathscr{V}$ there exists the natural symplectic structure

$$\omega^2 = d\mathbf{p} \wedge d\mathbf{q},$$

which is a closed, non-degenerate, differential two-form. We call the pair $(T^*\mathscr{V}, \omega^2)$ a symplectic manifold. The forms ω^2, $(\omega^2)^2$, ..., $(\omega^2)^N$ are preserved under both the phase flow of the system and under canonical transformations. Collectively, these forms are referred to as the Poincaré integral invariants. In fact,

0021-9991/91 $3.00

when integrated over an arbitrary region of dimension $2k$ $(1 \leqslant k \leqslant N)$, the $2k$-form ω^{2k} will produce the invariant quantity

$$\int \cdots^{2k} \int \sum_{i_1 < \cdots < i_k} dp_{i_1} \cdots dp_{i_k} \, dq_{i_1} \cdots dq_{i_k},$$

which is proportional to the sum of the oriented volumes of projections onto the coordinate spaces $(p_{i_1}, ..., p_{i_k}, q_{i_1}, ..., q_{i_k})$, where $1 \leqslant i_m \leqslant N$. When $k = N$, we recover Liouville's theorem.

A brief summary of existing symplectic integration algorithms (SIAs) is provided by Channell and Scovel [2]. In addition to the methods discussed there, Itoh and Abe [3] have recently developed a method of integration based on discrete mechanics which exactly preserves the Hamiltonian. Their algorithms, however, are accurate only up to second order in the time step and, like the schemes proposed by Channell and Scovel, require the solution of implicit equations. Ruth [4], however, has devised an explicit method of symplectic integration which is structurally quite similar to the classical Runge–Kutta algorithms (RKIs). In what follows, we generalize his approach and extend the accuracy of the method to fourth order in the time step. The resulting explicit SIA is superior in both computational efficiency and global stability to the most popular fourth-order RKI [5, 6].

This paper is divided into six sections. Section 2 explains the fundamental idea upon which our SIAs are based. Section 3 contains the actual derivation of explicit SIAs accurate to second, third, and fourth order in the time step. The generalization of the results to time-dependent potentials is accomplished in Section 4. Section 5 is devoted to the study of numerical examples and Section 6 contains a summary and discussion of results.

2. Approximate Canonical Transformations

Let us begin by considering a Hamiltonian $H: \mathscr{R}^N \times \mathscr{R}^N \to \mathscr{R}$ which is separable with respect to the local coordinates $\mathbf{q}$ and momenta $\mathbf{p}$,

$$H(\mathbf{q}, \mathbf{p}) = T(\mathbf{p}) + V(\mathbf{q}), \tag{1}$$

where $\mathbf{q} = \{q_\alpha\}$, $\mathbf{p} = \{p_\alpha\}$, $\alpha = 1, ..., N$. It is our goal to produce a series of difference equations which preserve the symplectic two-form $\omega^2 = d\mathbf{p} \wedge d\mathbf{q}$ and approximate the exact phase flow generated by H:

$$(\mathbf{q}_0, \mathbf{p}_0) \text{ at time } t_0 \to (\mathbf{q}, \mathbf{p}) \text{ at time } t. \tag{2}$$

The accuracy of the approximation resulting from replacing Hamilton's equations by such a series of difference equations will be measured in terms of the time step $\delta t = t - t_0$. More specifically, if a difference approximation agrees with Hamilton's

equations up to $O(\delta t^n)$, then we will call that approximation an nth order SIA. In what follows, let us consider $(\mathbf{q}_0, \mathbf{p}_0)$ to be initial conditions, and $(\mathbf{q}, \mathbf{p})$ to be the local coordinates and momenta after a time δt. Now, finding an nth order SIA is equivalent to finding a canonical transformation $\mathscr{C}$ which generates the map

$$\mathscr{C}: (\mathbf{q}, \mathbf{p}) \to (\tilde{\mathbf{q}}_0, \tilde{\mathbf{p}}_0) = (\mathbf{q}_0, \mathbf{p}_0) + O(\delta t^{n+1}), \tag{3}$$

where the tildes indicate approximate initial conditions. In particular, if we can find a series of transformations which leave the Hamiltonian with the final form

$$H(\tilde{\mathbf{q}}_0, \tilde{\mathbf{p}}_0) = \sum_{i=n}^{\infty} h_i(\tilde{\mathbf{q}}_0, \tilde{\mathbf{p}}_0)\, \delta t^i \tag{4}$$

such that $\tilde{\mathbf{q}}_0 \to \mathbf{q}_0$ and $\tilde{\mathbf{p}}_0 \to \mathbf{p}_0$ as $\delta t \to 0$, then one can prove that the equality in (3) is satisfied. Indeed, if we expand $(\tilde{\mathbf{q}}_0, \tilde{\mathbf{p}}_0)$ and $h_i(\tilde{\mathbf{q}}_0, \tilde{\mathbf{p}}_0)$ about $t = t_0$ in the following way,

$$(\tilde{\mathbf{q}}_0, \tilde{\mathbf{p}}_0) = (\mathbf{q}_0, \mathbf{p}_0) + \sum_{j=1}^{\infty} (\mathbf{q}^{(j)}, \mathbf{p}^{(j)})\, \delta t^j$$

$$h_i(\tilde{\mathbf{q}}_0, \tilde{\mathbf{p}}_0) = h_i(\mathbf{q}_0, \mathbf{p}_0) + O(\delta t)$$

then Hamilton's equations imply

$$\begin{aligned}\left(\frac{d}{dt}\tilde{\mathbf{q}}_0, \frac{d}{dt}\tilde{\mathbf{p}}_0\right) &= \sum_{i=n}^{\infty} \left(\frac{\partial}{\partial \tilde{\mathbf{p}}_0}, -\frac{\partial}{\partial \tilde{\mathbf{q}}_0}\right) h_i(\tilde{\mathbf{q}}_0, \tilde{\mathbf{p}}_0)\, \delta t^i \\ &= \delta t^n \left[\left(\frac{\partial}{\partial \tilde{\mathbf{p}}_0}, -\frac{\partial}{\partial \tilde{\mathbf{q}}_0}\right) h_n\right]_{\tilde{\mathbf{q}}_0 = \mathbf{q}_0,\ \tilde{\mathbf{p}}_0 = \mathbf{p}_0} + O(\delta t^{n+1}) \\ &= \mathbf{G}(\mathbf{q}_0, \mathbf{p}_0)\, \delta t^n + O(\delta t^{n+1}),\end{aligned}$$

where $\mathbf{G}$ is some vector function of the initial conditions. Upon integration of the above results, we obtain the relationship between the exact and approximate initial conditions,

$$(\tilde{\mathbf{q}}_0, \tilde{\mathbf{p}}_0) = (\mathbf{q}_0, \mathbf{p}_0) + \frac{\mathbf{G}}{n+1}\, \delta t^{n+1} + O(\delta t^{n+2}) \tag{5}$$

$$= (\mathbf{q}_0, \mathbf{p}_0) + O(\delta t^{n+1}). \tag{6}$$

One may conclude, then, that if a canonical transformation $\mathscr{C}$ (or a series of such transformations) transforms the Hamiltonian (1) into the form of (4), then the resulting algebraic equations of transformation constitute an nth-order SIA.

3. Development of Explicit Algorithms

We are now faced with the question: How does one transform a Hamiltonian (1) into the form (4)? Fortunately, this question has been answered by Ruth [4], who

has obtained explicit algorithms accurate to third order. This is in contrast to the recently developed implicit methods of Channell and Scovel [2] and of Itoh and Abe [3], which are somewhat less convenient for practical use in most cases.

3.1. *The Generating Functions*

To obtain an integration algorithm accurate to order n, we make the following series of l canonical transformations,

$$(\mathbf{q}_l, \mathbf{p}_l) \xrightarrow{K_l} (\mathbf{q}_{l-1}, \mathbf{p}_{l-1}) \xrightarrow{K_{l-1}} \cdots \xrightarrow{K_1} (\mathbf{q}_0, \mathbf{p}_0). \tag{7}$$

When $n \leqslant 4$, one can always set $l = n$. However, it may be necessary to use $l > n$ transformations when $n > 4$. This necessity is a result of the rapid accumulation with increasing n of independent conditions which must be satisfied to put H into the form (4). The reader familiar with classical Runge–Kutta formulae will recall a similar rise in the number of coefficients required to derive an algorithm of order greater than four. In any case, the above variables have the interpretation

$$\begin{aligned}
(\mathbf{q}_0, \mathbf{p}_0) &\rightarrow \text{initial conditions at time } t = 0 \\
(\mathbf{q}_1, \mathbf{p}_1) &\rightarrow \text{intermediate point} \\
&\vdots \\
(\mathbf{q}_{l-1}, \mathbf{p}_{l-1}) &\rightarrow \text{intermediate point} \\
(\mathbf{q}_l, \mathbf{p}_l) &\rightarrow \text{integrated variables at time } t = t_0 + \delta t
\end{aligned}$$

and

$$K_i(\mathbf{q}_{i-1}, \mathbf{p}_i, t) = -\mathbf{q}_{i-1} \cdot \mathbf{p}_i - [a_i T(\mathbf{p}_i) + b_i V(\mathbf{q}_{i-1})]\, \delta t \tag{8}$$

are type 3 generating functions for $i = 1, ..., l$. This choice of K_i yields the equations of transformation

$$\mathbf{q}_i = -\nabla_{\mathbf{p}_i} K_i = \mathbf{q}_{i-1} + \delta t a_i \nabla_{\mathbf{p}_i} T(\mathbf{p}_i) \tag{9}$$

$$\mathbf{p}_{i-1} = -\nabla_{\mathbf{q}_{i-1}} K_i = \mathbf{p}_i + \delta t b_i \nabla_{\mathbf{q}_{i-1}} V(\mathbf{q}_{i-1}) \tag{10}$$

and

$$H_{i-1}(\mathbf{q}_{i-1}, \mathbf{p}_{i-1}) = H_i + \partial_t K_i = H_i - [a_i T(\mathbf{p}_i) + b_i V(\mathbf{q}_{i-1})], \tag{11}$$

again, for $i = 1, ..., l$. The gradient operators we use here are defined according to

$$\nabla_{\mathbf{q}} \equiv \left(\frac{\partial}{\partial q_1}, ..., \frac{\partial}{\partial q_N} \right)$$

$$\nabla_{\mathbf{p}} \equiv \left(\frac{\partial}{\partial p_1}, ..., \frac{\partial}{\partial p_N} \right).$$

Upon applying all l transformations, it is clear that the Hamiltonian for the initial conditions, H_0, will have the form

$$H_0(\mathbf{q}_0, \mathbf{p}_0) = H_l(\mathbf{q}_l, \mathbf{p}_l) + \sum_{i=1}^{l} \partial_t K_i$$

$$= T(\mathbf{p}_l) + V(\mathbf{q}_l) - \sum_{i=1}^{l} [a_i T(\mathbf{p}_i) + b_i V(\mathbf{q}_{i-1})], \tag{12}$$

where in the above we must consider $\mathbf{q}_i = \mathbf{q}_i(\mathbf{q}_0, \mathbf{p}_0)$ and $\mathbf{p}_i = \mathbf{p}_i(\mathbf{q}_0, \mathbf{p}_0)$. At the moment, however, the relationships between variables are implicit, the exact form of which follows at once from the equations of transformation (9) and (10),

$$\mathbf{q}_i = \mathbf{q}_0 + \delta t \sum_{m=1}^{i} a_m \mathbf{P}(\mathbf{p}_m) \tag{13}$$

$$\mathbf{p}_i = \mathbf{p}_0 + \delta t \sum_{m=1}^{i} b_m \mathbf{F}(\mathbf{q}_{m-1}), \tag{14}$$

true for $i = 1, ..., l$. Note that we have introduced the generalized force $\mathbf{F}(\mathbf{q}) = -\nabla_{\mathbf{q}} V(\mathbf{q})$, as well as the gradient of kinetic energy $\mathbf{P}(\mathbf{p}) = \nabla_{\mathbf{p}} T(\mathbf{p})$. Now, if one can determine the coefficients $\{a_i, b_i\}$ such that the Hamiltonian has the form $H_0 = O(\delta t^n)$, then (9) and (10) describe an l-step process for the integration $(\mathbf{q}_0, \mathbf{p}_0) \to (\mathbf{q}_l, \mathbf{p}_l)$ which is exactly symplectic (since it is always a canonical transformation). In practice, to determine the coefficients $\{a_i, b_i\}$, one must expand $\mathbf{q}_i$ and $\mathbf{p}_i$, and all associated functions of in powers of δt so that H_0 may take the form

$$H_0(\mathbf{q}_0, \mathbf{p}_0) = \sum_{m=0}^{n-1} h_m(\{a_i, b_i\}, \mathbf{q}_0, \mathbf{p}_0)\, \delta t^m + O(\delta t^n), \tag{15}$$

in which case $\{a_i, b_i\}$ are found, not necessarily uniquely, by setting $h_m = 0$ for $m = 0, ..., n-1$.

3.2. *Series Expansions for* $n \leqslant 4$

Let us now perform the required algebra to find a fourth-order algorithm. Since methods of order 1, 2, and 3 are simpler cases of the order 4 method, we shall not yet specify the number $l = n \leqslant 4$ of transformations. First, we expand $\mathbf{q}_i$ and $\mathbf{p}_i$ in powers of δt,

$$\mathbf{q}_i = \mathbf{q}_0 + \delta t \boldsymbol{\Gamma}_i + \delta t^2 \boldsymbol{\Lambda}_i + \delta t^3 \boldsymbol{\Psi}_i + O(\delta t^4) \tag{16}$$

$$\mathbf{p}_i = \mathbf{p}_0 + \delta t \boldsymbol{\Theta}_i + \delta t^2 \boldsymbol{\Phi}_i + \delta t^3 \boldsymbol{\Pi}_i + O(\delta t^4) \tag{17}$$

with the coefficients given by

$$\boldsymbol{\Gamma}_i = \mathbf{P} \sum_{m=1}^{i} a_m$$

$$\boldsymbol{\Lambda}_i = (\mathbf{F} \cdot \nabla_{\mathbf{p}})\, \mathbf{P} \sum_{m=1}^{i} a_m \sum_{r=1}^{m} b_r$$

$$\Psi_i = \frac{(\mathbf{F}\cdot\nabla_{\mathbf{p}})^2}{2}\mathbf{P}\sum_{m=1}^{i} a_m\left[\sum_{r=1}^{m} b_r\right]^2 + [((\mathbf{P}\cdot\nabla_{\mathbf{q}})\mathbf{F})\cdot\nabla_{\mathbf{p}}]\mathbf{P}\sum_{m=2}^{i} a_m \sum_{r=2}^{m} b_r \sum_{s=1}^{r-1} a_s$$

$$\Theta_i = \mathbf{F}\sum_{m=1}^{i} b_m$$

$$\Phi_i = (\mathbf{P}\cdot\nabla_{\mathbf{p}})\mathbf{F}\sum_{m=2}^{i} b_m \sum_{r=1}^{m-1} a_r$$

$$\Pi_i = \frac{(\mathbf{P}\cdot\nabla_{\mathbf{q}})^2}{2}\mathbf{F}\sum_{m=2}^{i} b_m\left[\sum_{r=1}^{m-1} a_r\right]^2 + [((\mathbf{F}\cdot\nabla_{\mathbf{p}})\mathbf{P})\cdot\nabla_{\mathbf{q}}]\mathbf{F}\sum_{m=2}^{i} b_m \sum_{r=1}^{m-1}{}_{r}\sum_{s=1}^{r} b_s.$$

The coefficients above are evaluated, after application of the gradient operators, at $\mathbf{q}=\mathbf{q}_0$ and $\mathbf{p}=\mathbf{p}_0$. That is, they are explicit functions of the *initial conditions only*. Further, they are valid for $i=1, \ldots, n$. In a similar manner, we can expand $V(\mathbf{q}_i)$ and $T(\mathbf{p}_i)$:

$$V(\mathbf{q}_i) = V(\mathbf{q}_0) + \delta t[\boldsymbol{\Gamma}_i\cdot\nabla_{\mathbf{q}}]\,V(\mathbf{q}) + \delta t^2\left[\boldsymbol{\Lambda}_i\cdot\nabla_{\mathbf{q}} + \frac{(\boldsymbol{\Gamma}_i\cdot\nabla_{\mathbf{q}})^2}{2}\right]V(\mathbf{q}) + \delta t^3\left[\boldsymbol{\Psi}_i\cdot\nabla_{\mathbf{q}} + \frac{(\boldsymbol{\Gamma}_i\cdot\nabla_{\mathbf{q}})^3}{6} + (\boldsymbol{\Gamma}_i\cdot\nabla_{\mathbf{q}})(\boldsymbol{\Lambda}_i\cdot\nabla_{\mathbf{q}})\right]V(\mathbf{q}) + O(\delta t^4) \tag{18}$$

and

$$T(\mathbf{p}_i) = T(\mathbf{p}_0) + \delta t[\boldsymbol{\Theta}_i\cdot\nabla_{\mathbf{p}}]\,T(\mathbf{p}) + \delta t^2\left[\boldsymbol{\Phi}_i\cdot\nabla_{\mathbf{p}} + \frac{(\boldsymbol{\Theta}_i\cdot\nabla_{\mathbf{p}})^2}{2}\right]T(\mathbf{p}) + \delta t^3\left[\boldsymbol{\Pi}_i\cdot\nabla_{\mathbf{p}} + \frac{(\boldsymbol{\Theta}_i\cdot\nabla_{\mathbf{p}})^3}{6} + (\boldsymbol{\Theta}_i\cdot\nabla_{\mathbf{p}})(\boldsymbol{\Phi}_i\cdot\nabla_{\mathbf{p}})\right]T(\mathbf{p}) + O(\delta t^4). \tag{19}$$

Again, after the derivatives are taken, these expressions are evaluated at the initial conditions $(\mathbf{q}_0, \mathbf{p}_0)$. Upon substitution of the above expressions into (12), we arrive at a Hamiltonian with the form (15)

$$H_0(\mathbf{q}_0, \mathbf{p}_0) = h_0 + h_1\,\delta t + h_2\,\delta t^2 + h_3\,\delta t^3 + O(\delta t^4), \tag{20}$$

where the zero-order term is

$$h_0 = T(\mathbf{p}_0)\left[1 - \sum_{i=1}^{n} a_i\right] + V(\mathbf{q}_0)\left[1 - \sum_{i=1}^{n} b_i\right].$$

To avoid possible confusion, we will abbreviate $\mathbf{F}_0 = \mathbf{F}(\mathbf{q}_0)$ and $\mathbf{P}_0 = \mathbf{P}(\mathbf{p}_0)$. This allows us to write

$$h_1 = (\mathbf{F}_0 \cdot \mathbf{P}_0)\left[\sum_{m=1}^{n} b_m - \sum_{i=1}^{n} a_i \sum_{m=1}^{i} b_m - \sum_{m=1}^{n} a_m + \sum_{i=2}^{n} b_i \sum_{m=1}^{i-1} a_m\right]$$

and

$$\begin{aligned} h_2 = {} & (\mathbf{P}_0 \cdot \nabla_{\mathbf{q}})(\mathbf{F} \cdot \mathbf{P}_0)\left[\sum_{m=2}^{n} b_m \sum_{r=1}^{m-1} a_r - \sum_{i=2}^{n} a_i \sum_{m=2}^{i} b_m \sum_{r=1}^{m-1} a_r \right. \\ & \left. - \frac{1}{2}\left(\sum_{m=1}^{n} a_m\right)^2 + \frac{1}{2}\sum_{i=2}^{n} b_i \left(\sum_{m=1}^{i-1} a_m\right)^2\right] \\ & - (\mathbf{F}_0 \cdot \nabla_{\mathbf{p}})(\mathbf{P} \cdot \mathbf{F}_0)\left[\sum_{m=1}^{n} a_m \sum_{r=1}^{m} b_r - \sum_{i=2}^{n} b_i \sum_{m=1}^{i-1} a_m \sum_{r=1}^{m} b_r \right. \\ & \left. - \frac{1}{2}\left(\sum_{m=1}^{n} b_m\right)^2 + \frac{1}{2}\sum_{i=1}^{n} a_i \left(\sum_{m=1}^{i} b_m\right)^2\right]. \end{aligned}$$

It can be shown, finally, that h_3 has the following lengthy expansion,

$$\begin{aligned} h_3 = {} & (\mathbf{P}_0 \cdot \nabla_{\mathbf{q}})^2 (\mathbf{F} \cdot \mathbf{P}_0)\left[\frac{1}{2}\sum_{m=2}^{n} b_m \left(\sum_{r=1}^{m-1} a_r\right)^2 \right. \\ & \left. - \frac{1}{2}\sum_{i=2}^{n} a_i \sum_{m=2}^{i} b_m \left(\sum_{r=1}^{m-1} a_r\right)^2 - \frac{1}{6}\left(\sum_{m=1}^{n} a_m\right)^3 + \frac{1}{6}\sum_{i=2}^{n} b_i \left(\sum_{m=1}^{i-1} a_m\right)^3\right] \\ & - (\mathbf{F}_0 \cdot \nabla_{\mathbf{p}})^2 (\mathbf{P} \cdot \mathbf{F}_0)\left[\frac{1}{2}\sum_{m=1}^{n} a_m \left(\sum_{r=1}^{m} b_r\right)^2 \right. \\ & \left. - \frac{1}{2}\sum_{i=2}^{n} b_i \sum_{m=1}^{i-1} a_m \left(\sum_{r=1}^{m} b_r\right)^2 - \frac{1}{6}\left(\sum_{m=1}^{n} b_m\right)^3 + \frac{1}{6}\sum_{i=1}^{n} a_i \left(\sum_{m=1}^{i} b_m\right)^3\right] \\ & + (\mathbf{P}_0 \cdot \nabla_{\mathbf{q}})(\mathbf{F}_0 \cdot \nabla_{\mathbf{p}})(\mathbf{P} \cdot \mathbf{F})\left[\sum_{m=2}^{n} b_m \sum_{r=1}^{m-1} a_r \sum_{s=1}^{r} b_s - \sum_{m=2}^{n} a_m \sum_{r=2}^{m} b_r \sum_{s=1}^{r-1} a_s \right. \\ & - \sum_{i=2}^{n} a_i \sum_{m=2}^{i} b_m \sum_{r=1}^{m-1} a_r \sum_{s=1}^{r} b_s + \sum_{i=3}^{n} b_i \sum_{m=2}^{i-1} a_m \sum_{r=2}^{m-1} b_r \sum_{s=1}^{r-1} a_s \\ & + \sum_{m=1}^{n} b_m \sum_{m=2}^{n} b_m \sum_{r=1}^{m-1} a_r - \sum_{i=2}^{n} a_i \sum_{m=1}^{i} b_m \sum_{m=2}^{i} b_m \sum_{r=1}^{m-1} a_r \\ & \left. - \sum_{m=1}^{n} a_m \sum_{m=1}^{n} a_m \sum_{r=1}^{m} b_r + \sum_{i=2}^{n} b_i \sum_{m=1}^{i-1} a_m \sum_{r=1}^{m} b_r\right]. \end{aligned}$$

As before, each of the expressions $h_0, \ldots, h_3$ is to be evaluated at the initial conditions $(\mathbf{q}_0, \mathbf{p}_0)$. Using the results we have derived so far, it is possible to derive algorithms of orders 1, 2, 3, and 4 by making the choices shown in Table I. The

TABLE I

Summary of Different Choices of Algorithms

Order	Equate to zero	n	Equations	Variables
1	h_0	1	2	2
2	h_0, h_1	2	3	4
3	h_0, h_1, h_2	3	5	6
4	h_0, h_1, h_2, h_3	4	8	8

coefficients which result from these choices are listed in Table II. Once the coefficients $\{a_i, b_i\}$ are known, we have the prescription shown in Table III for an nth-order integrator. Of course, algorithms of order $\leqslant 3$ have been derived by Ruth [4], but we will include a general treatment of them for completeness. The case $n=1$ is trivial, but for $n=2$, one obtains the so-called *leapfrog* method which we will derive in the next section.

3.3. *A Second-Order SIA*

According to Table I, if we set h_0 and h_1 equal to zero and choose $n=2, 3$ equations in four variables result:

$$a_1 + a_2 = 1 \tag{21}$$

$$b_1 + b_2 = 1 \tag{22}$$

$$a_1 b_1 + a_2 = b_2 a_1. \tag{23}$$

Two particularly interesting solutions are the *leapfrog* method

$$(a_1, a_2, b_1, b_2) = (\tfrac{1}{2}, \tfrac{1}{2}, 0, 1),$$

and the *pseudo-leapfrog* method

$$(a_1, a_2, b_1, b_2) = (1, 0, \tfrac{1}{2}, \tfrac{1}{2}).$$

TABLE II

Summary of Coefficients for Various Algorithms

Order (n)	Coefficients
1	$(a_1, b_1) = (1, 1)$
2	$(a_1, a_2, b_1, b_2) = (\frac{1}{2}, \frac{1}{2}, 0, 1)$
3	$(a_1, a_2, a_3, b_1, b_2, b_3) = (\frac{2}{3}, -\frac{2}{3}, 1, \frac{7}{24}, \frac{3}{4}, -\frac{1}{24})$
4	$a_1 = a_4 = \frac{1}{6}(2 + 2^{1/3} + 2^{-1/3})$ $a_2 = a_3 = \frac{1}{6}(1 - 2^{1/3} - 2^{-1/3})$ $b_1 = 0$ $b_2 = b_4 = (2 - 2^{1/3})^{-1}$ $b_3 = (1 - 2^{2/3})^{-1}$

TABLE III

General Scheme for a δt Time-Step Integration

Hamiltonian: $H(\mathbf{q}, \mathbf{p}) = T(\mathbf{p}) + V(\mathbf{q})$
Initial conditions: $(\mathbf{q}_0, \mathbf{p}_0)$ at $t = t_0$
Do for $i = 1$ to n: $\mathbf{p}_i = \mathbf{p}_{i-1} + b_i \mathbf{F}(\mathbf{q}_{i-1})\,\delta t$, $\mathbf{q}_i = \mathbf{q}_{i-1} + a_i \mathbf{P}(\mathbf{p}_i)\,\delta t$
Integrated variables: $(\mathbf{q}_n, \mathbf{p}_n)$ at $t = t_0 + \delta t$

These coefficients are implemented into a numerical integration scheme according to Table III.

3.4. *A Third-Order SIA*

In this case $n = 3$ and h_0, h_1, h_2 must be set equal to zero. One is then left with five equations in six variables:

$$a_1 + a_2 + a_3 = 1 \tag{24}$$

$$b_1 + b_2 + b_3 = 1 \tag{25}$$

$$b_2 a_1 + b_3 (a_1 + a_2) = \tfrac{1}{2} \tag{26}$$

$$a_1 b_1^2 + a_2 (b_1 + b_2)^2 + a_3 = \tfrac{1}{3} \tag{27}$$

$$b_2 a_1^2 + b_3 (a_1 + a_2)^2 = \tfrac{1}{3}. \tag{28}$$

A solution found originally by Ruth [4] is

$$(a_1, a_2, a_3, b_1, b_2, b_3) = (\tfrac{2}{3}, -\tfrac{2}{3}, 1, \tfrac{7}{24}, \tfrac{3}{4}, -\tfrac{1}{24}).$$

Again, these coefficients are implemented according to the procedure in Table III.

3.5. *A Fourth-Order SIA*

One of the most popular methods used for numerical integration of differential equations is the fourth-order RKI shown in Appendix 1. However, this RKI is not symplectic, and requires four evaluations of the force **F** per time step. The SIA that we will now present requires only three evaluations of the force per time step, and, because of its canonical nature, preserves more accurately global phase space structures. Setting h_0, h_1, h_2, and h_3 equal to zero yields eight equations in eight variables:

$$a_1 + a_2 + a_3 + a_4 = 1 \tag{29}$$

$$b_1 + b_2 + b_3 + b_4 = 1 \tag{30}$$

$$b_2 a_1 + b_3 (a_1 + a_2) + b_4 (1 - a_4) = \tfrac{1}{2} \tag{31}$$

$$a_1 b_1^2 + a_2(b_1 + b_2)^2 + a_3(1 - b_4)^2 + a_4 = \tfrac{1}{3} \tag{32}$$

$$b_2 a_1^2 + b_3(a_1 + a_2)^2 + b_4(1 - a_4)^2 = \tfrac{1}{3} \tag{33}$$

$$a_1 b_1^3 + a_2(b_1 + b_2)^3 + a_3(1 - b_4)^3 + a_4 = \tfrac{1}{4} \tag{34}$$

$$b_2 a_1^3 + b_3(a_1 + a_2)^3 + b_4(1 - a_4)^3 = \tfrac{1}{4} \tag{35}$$

$$\begin{aligned} b_2 a_1 + b_3(a_1 + a_2)[a_1 b_1 + a_2(b_1 + b_2)] + b_4(1 - a_4)[\tfrac{1}{2} - a_4] \\ = a_2(b_1 + b_2)[b_2 a_1] + a_3(1 - b_4)[\tfrac{1}{2} - b_4(1 - a_4)] + \tfrac{1}{2} a_4. \end{aligned} \tag{36}$$

It can be shown that the following is an analytic solution of the equations

$$\begin{aligned} a_1 = a_4 &= \tfrac{1}{6}(2 + 2^{1/3} + 2^{-1/3}) \\ a_2 = a_3 &= \tfrac{1}{6}(1 - 2^{1/3} - 2^{-1/3}) \\ b_1 &= 0 \\ b_2 = b_4 &= \frac{1}{2 - 2^{1/3}} \\ b_3 &= \frac{1}{1 - 2^{2/3}}. \end{aligned}$$

A similar solution exists for which only three evaluations of $\mathbf{P}$ are necessary.

4. Time-Dependent Potentials

The case where the potential V is an explicit function of time is easily accounted for. Let us begin by assuming we have a Hamiltonian $H: \mathscr{R}^N \times \mathscr{R}^N \times \mathscr{R} \to \mathscr{R}$,

$$H(\mathbf{q}, \mathbf{p}, t) = T(\mathbf{p}) + V(\mathbf{q}, t). \tag{37}$$

If we define the type 1 generating function $\mathscr{F} = p_\varphi t$, then time can be eliminated by introducing the canonically conjugate pair (φ, p_φ). The equations of transformation are

$$\varphi = \frac{\partial \mathscr{F}}{\partial p_\varphi} = t \tag{38}$$

$$H_{\text{new}} = H + \partial_t \mathscr{F} = H + p_\varphi. \tag{39}$$

Note that φ is numerically equal to t and that $p_\varphi = -H(\mathbf{q}, \mathbf{p}, t) + \text{constant}$. Upon substitution, we find

$$H_{\text{new}}(\mathbf{q}, \varphi, \mathbf{p}, p_\varphi) = [T(\mathbf{p}) + p_\varphi] + V(\mathbf{q}, \varphi), \tag{40}$$

which is equivalent to (1), but extended to $N+1$ degrees of freedom. Table IV shows the prescription for integrating the equations of motion corresponding to the Hamiltonian (37), with the generalized force defined by $\mathbf{F}(\mathbf{q}, t) = -\nabla_{\mathbf{q}} V(\mathbf{q}, t)$.

5. Numerical Examples

All numerical calculations quoted in this paper were done using a version of VAX FORTRAN which was compiled and run on a DEC MicroVAX II computer. The double-precision (REAL*8) format was used for all floating point numbers since the accuracy of single-precision (REAL*4) variables is insufficient for long-time numerical integration.

5.1. *The Nonlinear Pendulum*

Our first example is the nonlinear pendulum, which is described by the following Hamiltonian

$$H(q, p) = \frac{p^2}{2} - \cos q. \tag{41}$$

The solutions for $q(t)$ and $p(t)$ are well known and can be expressed in terms of Jacobian elliptic functions [7]. If we impose the initial conditions $q(0) = 0$ and $p(0) = p_0$, then

$$q(t) = 2 \operatorname{am}\left(\frac{t}{k}, k\right)$$

$$p(t) = \pm\frac{2}{k} \operatorname{dn}\left(\frac{t}{k}, k\right),$$

where $k^2 = 4/p_0^2$. Using these analytical results, we were able to monitor exactly the errors in p and q, as well as the error in energy. The RKIs which we shall use for comparitive purposes are listed in Appendix 1. For the sake of brevity, the second-

TABLE IV

General Scheme for a δt Time-Step Integration

Hamiltonian: $H(\mathbf{q}, \mathbf{p}, t) = T(\mathbf{p}) + V(\mathbf{q}, t)$
Initial conditions: $(\mathbf{q}_0, \mathbf{p}_0)$ at $t = t_0$
Do for $i = 1$ to n:
$\mathbf{p}_i = \mathbf{p}_{i-1} + b_i \mathbf{F}(\mathbf{q}_{i-1}, t_{i-1})\,\delta t$, $\mathbf{q}_i = \mathbf{q}_{i-1} + a_i \mathbf{P}(\mathbf{p}_i)\,\delta t$
$t_i = t_{i-1} + a_i\,\delta t$
Integrated variables: $(\mathbf{q}_n, \mathbf{p}_n)$ at $t = t_0 + \delta t$

order Runge–Kutta method shall be called RKI2, and the fourth-order method RKI4. Similarly, the leapfrog method of Section 3.3 will hereby be referred to as SIA2, and the method of Section 3.5 will be called SIA4. Figures 1 and 2 compare the accuracy of SIA2 and RKI2, while Figs. 3 and 4 compare the accuracy of SIA4 and RKI4. In both cases, we see that the energy error for the SIAs is very small and tends to oscillate about some small central value, while the energy error for the RKIs increases monotonically. This characteristic has been noted by previous authors, most notably in [2].

The SIAs also reproduce the coordinate q more accurately than the RKIs. However, the symplectic methods show a higher rate of growth of coordinate error than of energy error. This phenomena is appropriately described as the propagation of a phase error [3] in the SIA.

5.2. *Particle in a Standing Wave Field*

The equation of motion

$$m\ddot{q} = -eE[\sin(kq - \omega t) + \sin(kq + \omega t)] \tag{42}$$

describes the motion of a particle of mass m, charge $-e$, in the field of a standing wave. Choosing units such that $\omega = k = m = 1$, we find that the above reduces to

$$\ddot{q} + \varepsilon \sin q \cos t = 0,$$

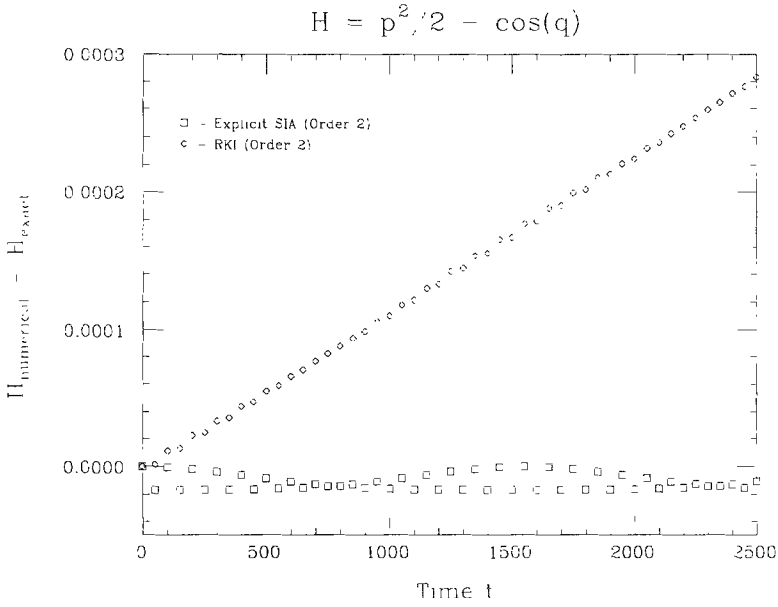

FIG. 1. Comparison of the relative error in energy when using SIA2 and RKI2 to integrate (41), with initial conditions $(q_0, p_0, t_0) = (0, 1.4, 0)$, and time step $\delta t = 0.01$.

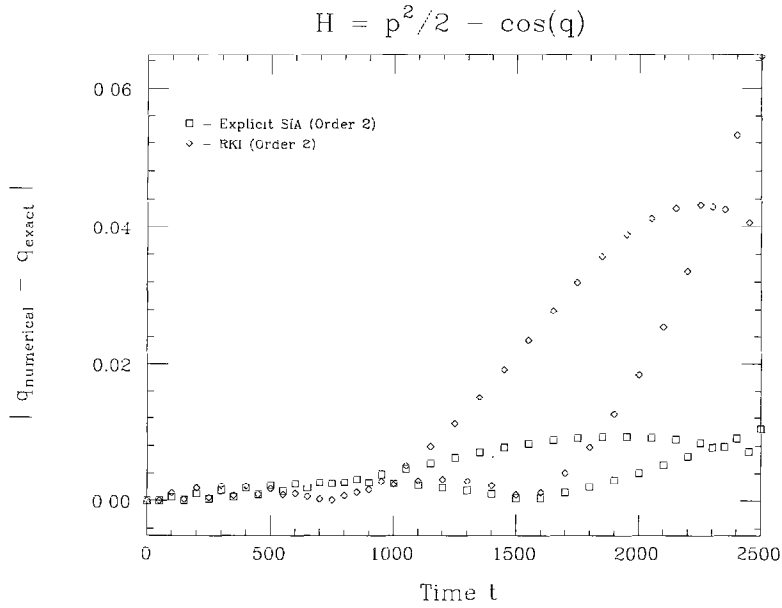

FIG. 2. Comparison of the absolute error in position when using SIA2 and RKI2 to integrate (41), with initial conditions $(q_0, p_0, t_0) = (0, 1.4, 0)$, and time step $\delta t = 0.01$.

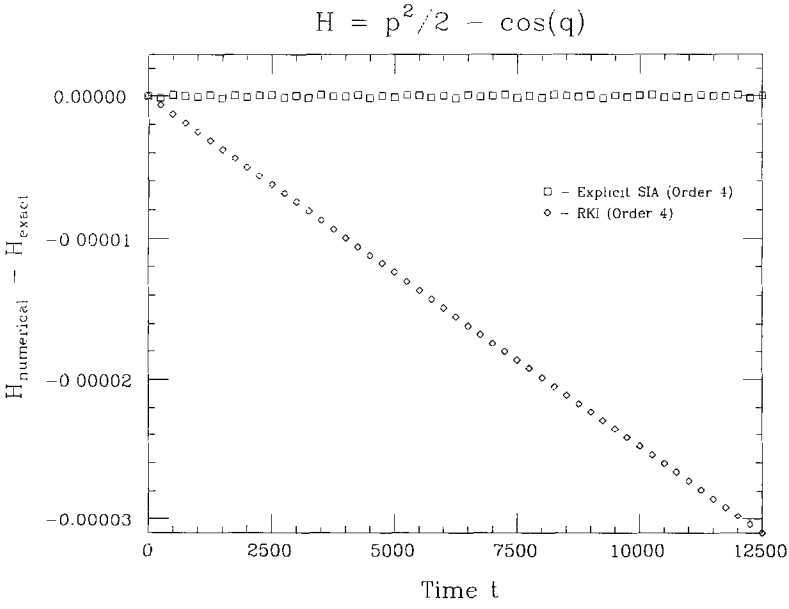

FIG. 3. Comparison of the relative error in energy when using SIA2 and RKI2 to integrate (41), with initial conditions $(q_0, p_0, t_0) = (0, 1.4, 0)$, and time step $\delta t = 0.05$.

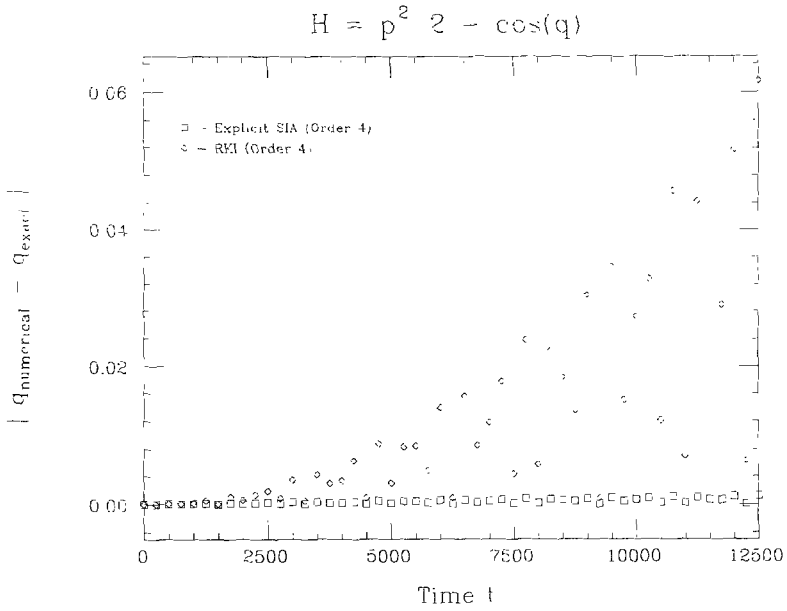

FIG. 4. Comparison of the absolute error in position when using SIA2 and RKI2 to integrate (41), with initial conditions $(q_0, p_0, t_0) = (0, 1.4, 0)$, and time step $\delta t = 0.05$.

where $\varepsilon = 2eE/m$. This equation is derivable from the time-dependent Hamiltonian function

$$H(q, p, t) = \frac{p^2}{2} - \varepsilon \cos q \cos t. \tag{43}$$

A crude estimate of the stochasticity threshold can be obtained by the resonance overlap criteria of Chirikov [8]. When $\varepsilon \geqslant \frac{1}{2}$, separatrices corresponding to each wave in (42) overlap, indicating that stochastic regions must be present in the phase

do indeed exist locally for values of ε much smaller than these estimates.

We begin the comparison by integrating the Hamiltonian (43) inside the ponderomotive potential well, and display the results at the times $t_m = 2\pi m$, $m = 0, 1, 2, ..., n$; where n is the total number of plotted points. This procedure defines our Poincaré return map. Comparing Fig. 6 and Fig. 7, we notice that SIA4 yields trajectories which lie on a well-defined submanifold while RKI4 seems to exhibit chaos. Actually, the unstable behavior of RKI4 in Fig. 7 is a result of its inability to accurately preserve the local constant of motion which defines the one-dimensional trajectory seen in Fig. 6. This numerical dissipation, which is also

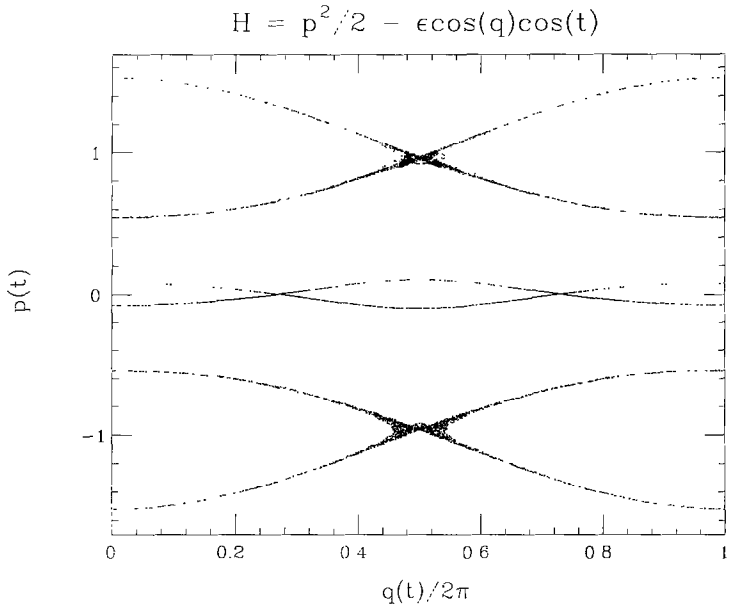

FIG. 5. Phase space of (43) for $\varepsilon = \frac{1}{8}$. The large separatrices at top and bottom correspond to resonance with the travelling waves in (42). The small, middle separatrix corresponds to the ponderomotive potential well.

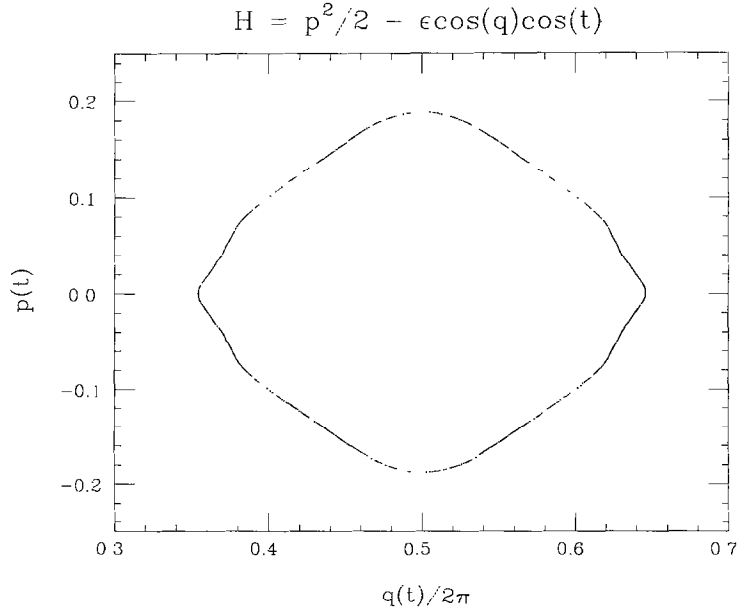

FIG. 6. Poincaré map of a single trajectory of (43) using SIA4. The initial conditions are $(q_0, p_0, t_0) = (\pi, 0.188, 0)$, $\varepsilon = 0.73/\pi \simeq 0.23$, $\delta t = 2\pi/25 \simeq 0.25$, with 30,000 plotted points.

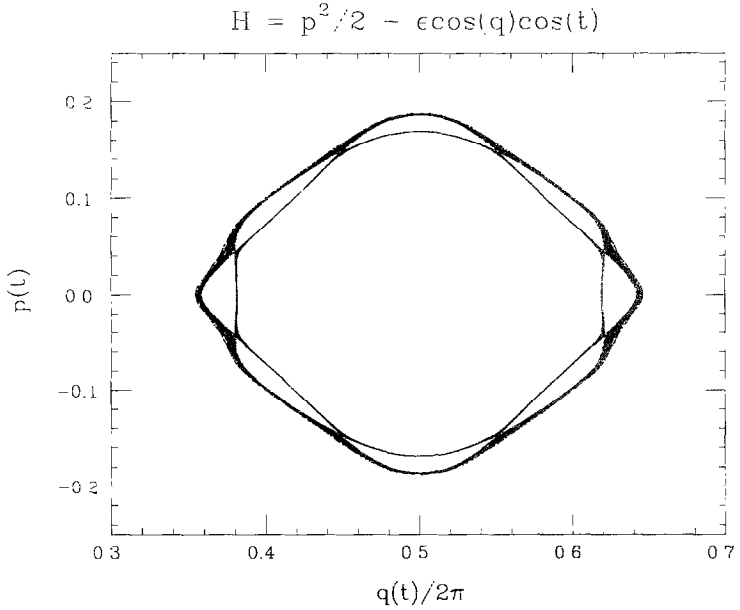

FIG. 7. Same as in Fig. 6, except using RKI4.

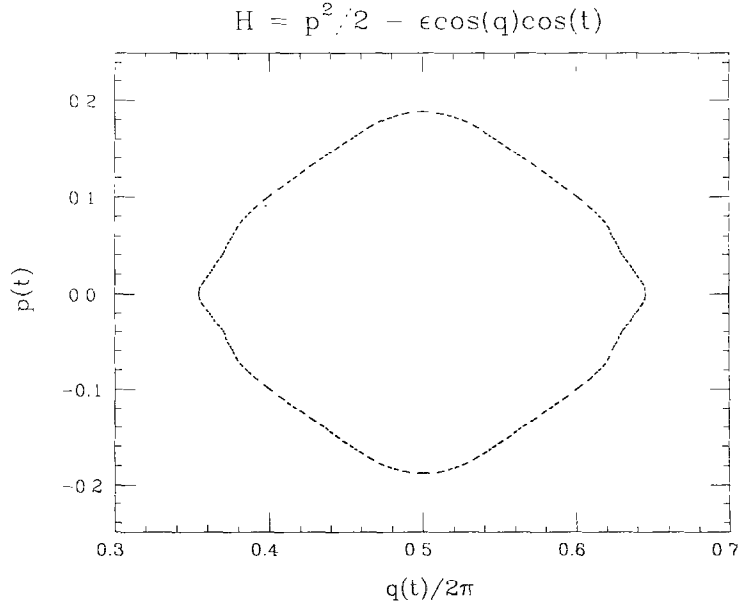

FIG. 8. Same as in Fig. 6, except using ISIA4.

TABLE V

Execution Time (in Seconds)
for Various Integration Methods

	$\delta t = 0.5$	$\delta t = 0.1$	$\delta t = 0.01$
SIA4	22.31	2.25	21.59
RKI4	31.79	31.74	30.88
ISIA4	42.64	32.77	26.69

evident in Fig. 3, causes RKI4 to be weakly attracted to the elliptic fixed point at $(q, p) = (\pi, 0)$. In addition, we have included in Fig. 8 the trajectories calculated using a fourth-order algorithm generated by the prescription in [2] (see Appendix 2), which we shall call ISIA4. As in the case of SIA4, ISIA4 shows a stable, regular trajectory.

An added consideration in the comparison of various methods is computational efficiency. Using the initial conditions $(q_0, p_0, t_0) = (\pi, 0.5, 0)$, and perturbation strength $\varepsilon = 1/4\pi \simeq 0.080$, we integrated the system corresponding to the Hamiltonian (43) forward in time $n = 10{,}000$ time steps. The results, using three different values of the time step δt, are shown in Table V. The FORTRAN source code for ISIA4 solved the implicit equation for the integrated coordinate according

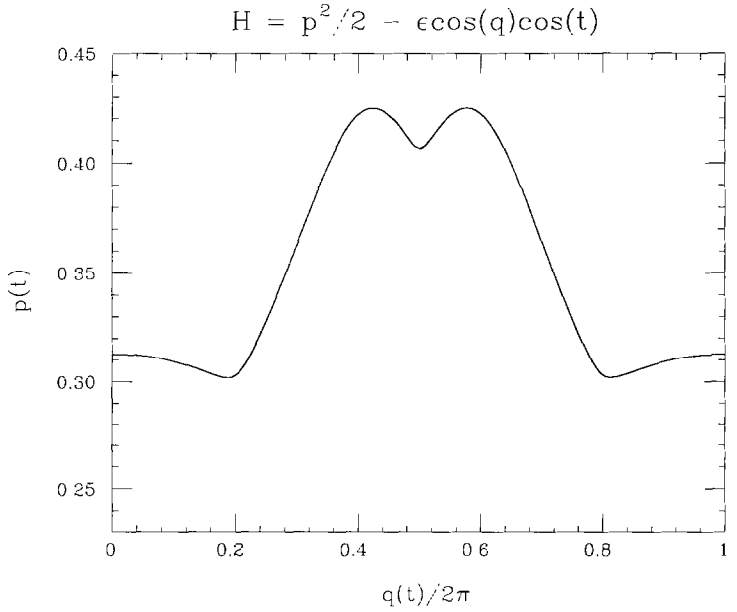

FIG. 9. Poincaré map of a single trajectory of (43) using SIA4. The initial conditions are $(q_0, p_0, t_0) = (0, 0.31255, 00)$, $\varepsilon = 1/2\pi \simeq 0.16$, $\delta t = 2\pi/30 \simeq 0.21$, with 30,000 plotted points.

to a simple fixed-point iteraton scheme with numerical accuracy $O(10^{-16})$. Other than this crude method of solution, the computer code was carefully optimized. As can be seen, ISIA4 benefits from having a small time step. In the next section, we will encounter a situation where the iteration scheme used in ISIA4 fails to converge.

A further example of the stability of SIA4 can be seen in Fig. 9, where the Poincaré map reveals the existence of a local constant of motion. In Fig. 10, however, we see that the equivalent trajectory calculated by RKI4 experiences numerical dissipation which eventually overwhelms the calculation. Interestingly, the difference between integrators is most easily noticed for regular trajectories of this sort. In the case when the motion is chaotic, the violation of topological invariants in phase space by Runge–Kutta methods is not so easily identified. Figures 11 and 12, which show the development of a stochastic layer in the vicinity of the ponderomotive potential well separatrix, illustrate this difficulty.

5.3. *Linear Oscillator Perturbed by a Plane Wave*

The motion of a charged particle in a constant magnetic field (directed along the z-axis) perturbed by a plane electrostatic wave (propogating along the x-axis) is described by the equation

$$\ddot{x} + \Omega^2 x = \varepsilon \sin(kx - \omega t). \tag{44}$$

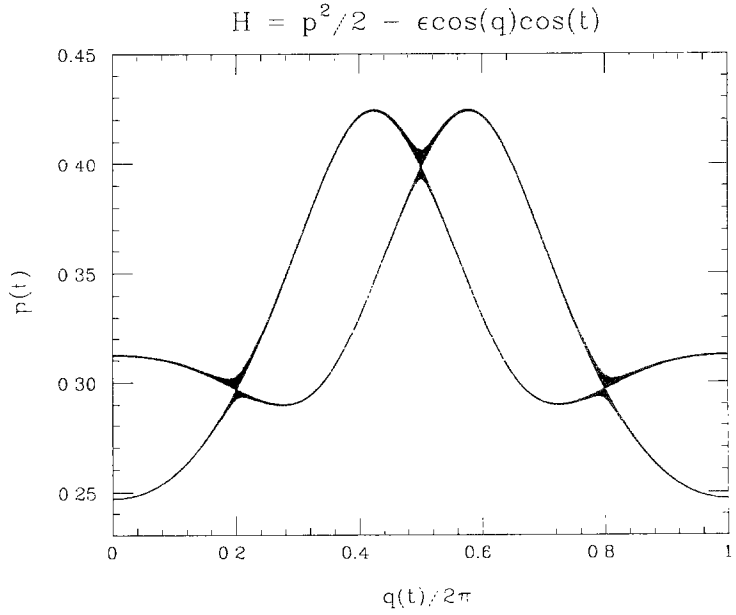

FIG. 10. Same as in Fig. 9, except using RKI4.

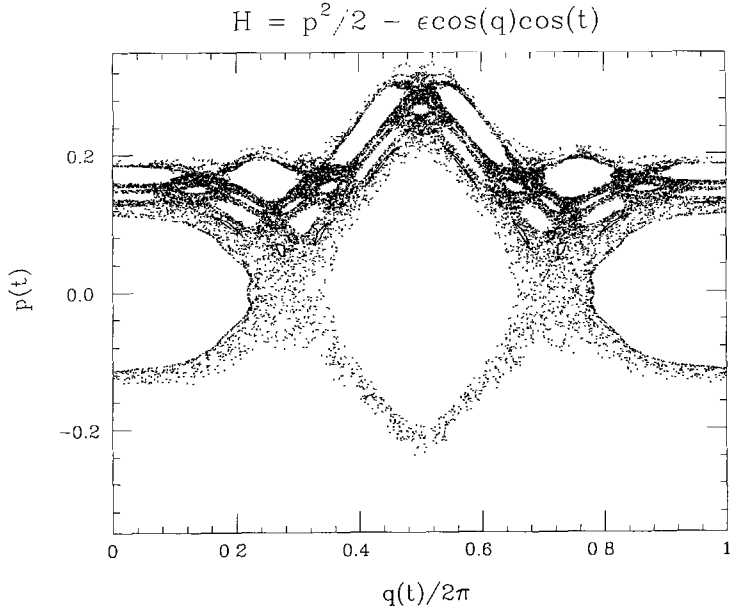

FIG.11. Poincaré map of a single trajectory of (43) using SIA4. The initial conditions are $(q_0, p_0, t_0) = (\pi, 0.255, 0)$, $\varepsilon = 0.73/\pi \simeq 0.23$, $\delta t = 2\pi/30 \simeq 0.21$, with 25,000 plotted points.

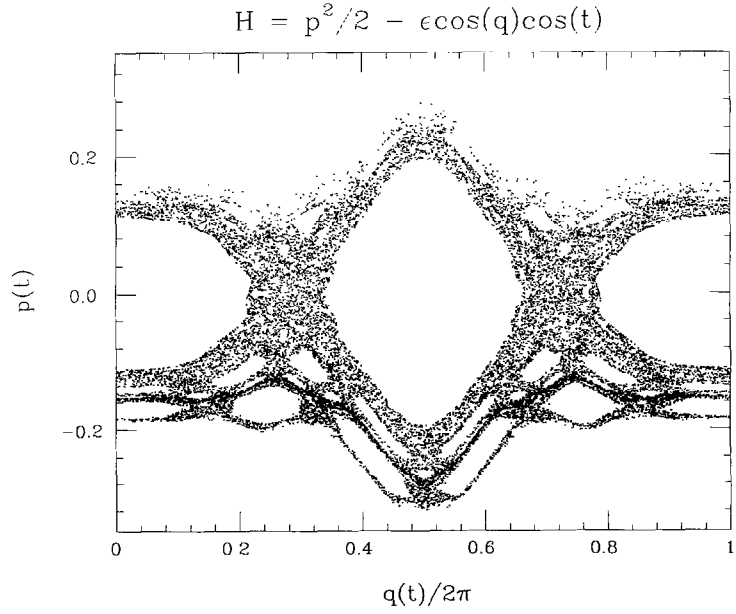

FIG. 12. Same as in Fig. 11, except using RKI4.

In this equation, Ω is the cyclotron frequncy and ω is the temporal frequency of the electrostatic wave. In the case of exact resonance $\omega = n\Omega$, Eq. (44) generates a stochastic web in phase space. Choosing units where $\Omega = k = 1$ and calling $q = x$, $p = \dot{x}$, (44) is easily seen to be derivable from the Hamiltonian

$$H(q, p, t) = \frac{p^2}{2} + \frac{q^2}{2} + \varepsilon \cos(q - \omega t), \tag{45}$$

where we shall assume ω is an integer, so that the resonance condition holds. This system has been studied by Chernikov *et al.* [10]. A slightly more general Hamiltonian,

$$H(q, p, t) = \frac{p^2}{2} + \frac{q^2}{2} + \varepsilon \sum_{i=1}^{s} \cos(q - \omega_i t), \tag{46}$$

describes the situation when there exist s perturbing electrostatic waves, each with the same wavenumber and amplitude, but with differing temporal frequencies ω_i. This more general system has been examined numerically by Murakami *et al.* [11].

First, we integrated the system corresponding to (45) for relatively small values of the parameter ε and $\omega = 7$. The Poincaré mappings were generated by plotting points at discrete times $t_m = 2\pi m/7$. Initial conditions were chosen with the particle on the separatrix net, with the results for SIA4 and RKI4 shown in Figs. 14 and 15,

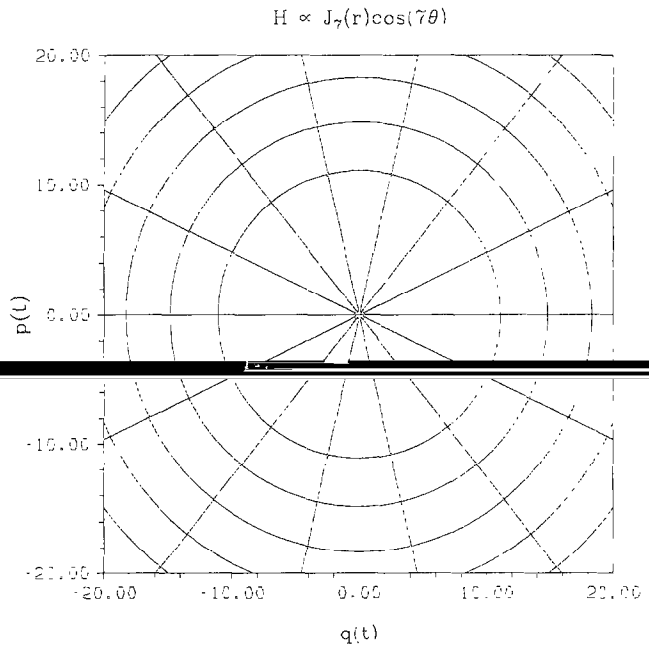

FIG. 13. Separatrix mesh of (45) after averaging, for $\omega = 7$ and $\varepsilon \ll 1$. The variables are defined by $r = \sqrt{q^2 + p^2}$ and $\tan\theta = p/q$.

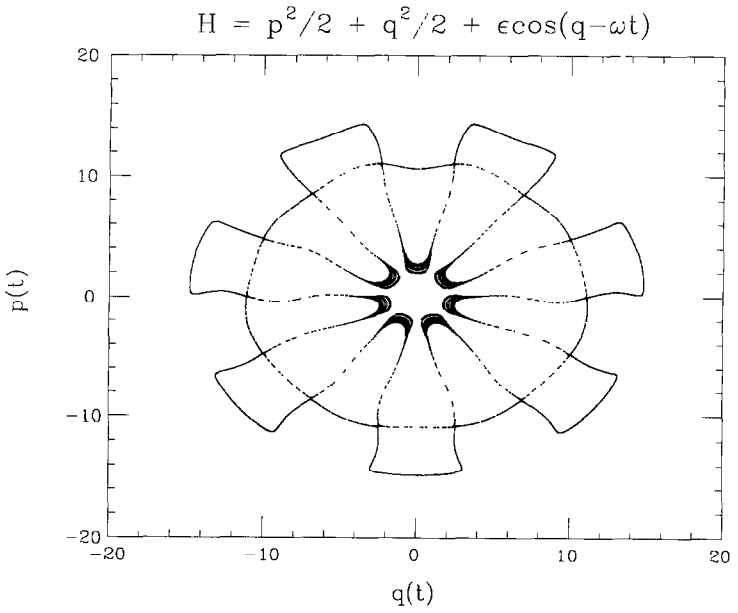

FIG. 14. Poincaré map of a single trajectory of (45) using SIA4. The initial conditions are $(q_0, p_0, t_0) = (0, 10.5939, 0)$, $\varepsilon = 0.8$, $\omega = 7$, $\delta t = 2\pi/63 \simeq 0.1$, with 35,000 plotted points.

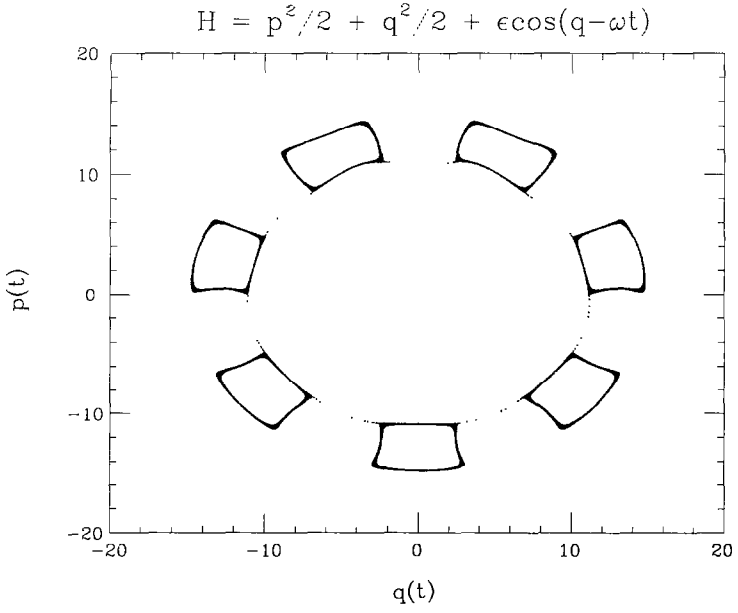

FIG. 15. Same as Fig. 14, except using RKI4.

respectively. These can be compared with the shape of the separatrix mesh (accurate to $O(\varepsilon)$) in Fig. 13, which can be obtained through averaging or perturbation methods (cf. Ref. [11]). This net is formed as a result of the intersection of resonant tori and can be shown to descrease in thickness rapidly with increasing particle velocity. Figure 14 shows the separatrix mesh traced by SIA4 to indeed be quite thin, even though the dynamics within the mesh is chaotic. Figure 15, on the other hand, shows RKI4 slowly spiralling into stable fixed points. Of physical interest for the Hamiltonian (45) is to what extent the particle can absorb energy from the electrostatic wave and be accelerated to high velocities. Determination of the possibility of such particle diffusion requires very long-time, high accuracy integrations. Any tendency of the integrator to become attracted to or repelled from stable equilibrium points will eventually manifest itself in the production of completely unphysical behavior. In this sense, the global stability properties of the SIAs make them well suited to such numerical experiments.

The lower order Runge–Kutta algorithm (RKI2) often tended to become wildly unstable even after a relatively small number of integration steps. To illustrate this tendency, we have included a comparison of SIA2 (Fig. 16) and RKI2 (Fig. 17). Much of the unstable behavior which we have noticed in the RKIs can be remedied by decreasing the size of δt. However, this only increases the length of the time-scale of valid behavior and ultimately comes at the expense of increased computational cost.

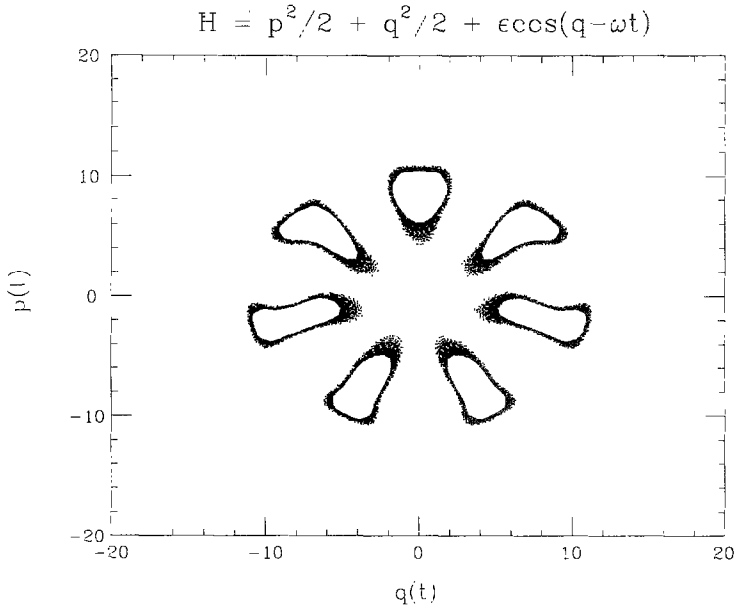

FIG. 16. Poincaré map of a single trajectory of (45) using SIA2. The initial conditions are $(q_0, p_0, t_0) = (0, 4.5, 0)$, $\varepsilon = 1.2$, $\omega = 7$, $\delta t = 2\pi/210 \simeq 0.03$, with 20,000 plotted points.

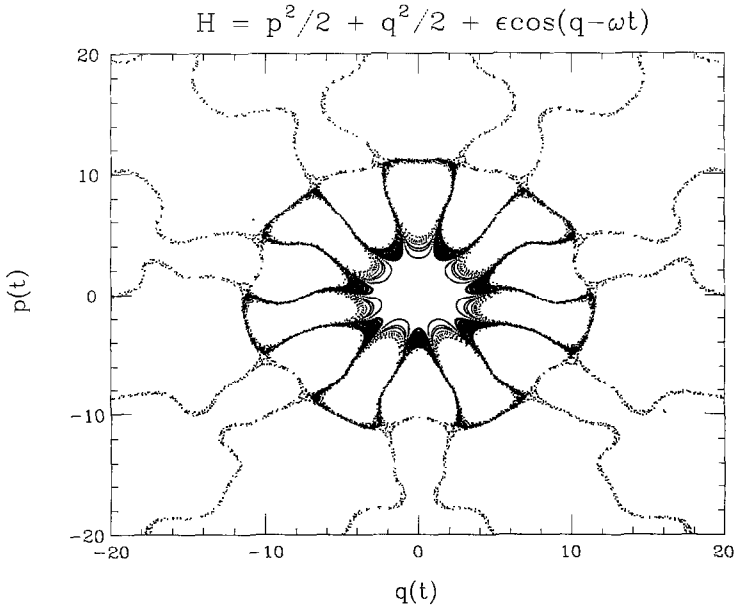

FIG. 17. Same as Fig. 16, except using RKI2.

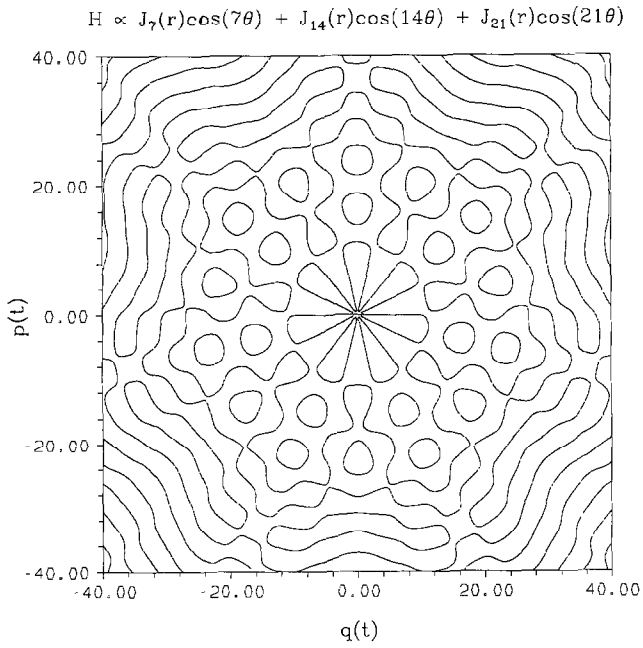

FIG. 18. Separatrix mesh of (46) after averaging, for $s=3$, $\omega_1=7$, $\omega_2=14$, $\omega_3=21$, and $\varepsilon \ll 1$. The variables are defined by $r=\sqrt{q^2+p^2}$ and $\tan\theta = p/q$.

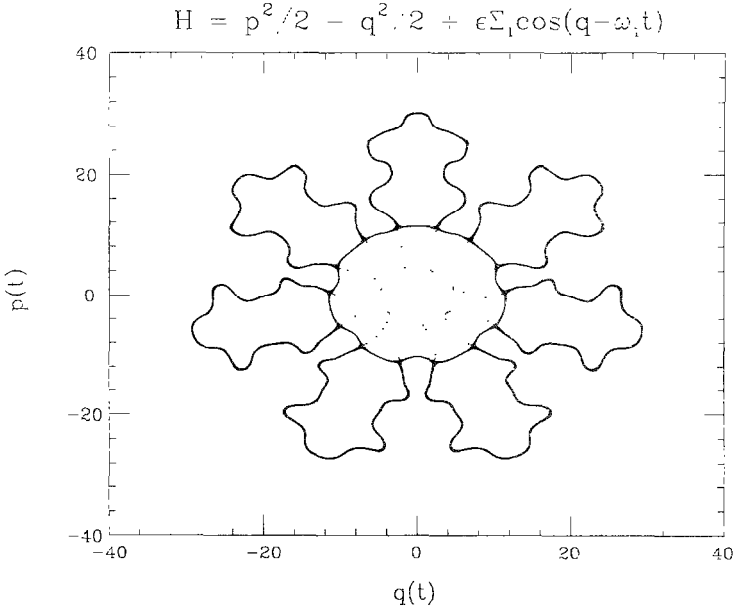

FIG. 19. Poincaré map of a single trajectory of (46) using SIA4. The initial conditions are $(q_0, p_0, t_0) = (0, 11.2075, 0)$, $\varepsilon = 1$, $s = 3$, $\omega_1 = 7$, $\omega_2 = 14$, $\omega_3 = 21$, $\delta t = 2\pi/105 \simeq 0.06$, with 38,000 plotted points.

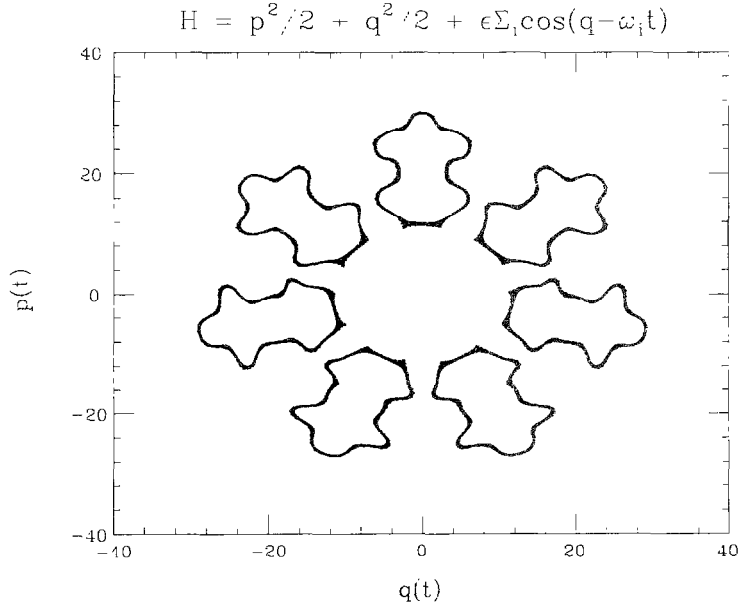

FIG. 20. Same as Fig. 19, except using RKI4.

As a final example of the web equation, we solve numerically the system described by (46), with $s=3$. The separatrix net of the averaged Hamiltonian is shown in Fig. 12, while the results obtained by SIA4 and RKI4 are shown in Figs. 18 and 19, respectively. Once again, the structure of the intersection of resonant tori is defined more sharply by SIA4 than by RKI4. An attempt to apply the implicit method of Channell and Scovel [2], in a manner similar to that of Section 3.2, resulted in divergence of the fixed-point iteration method used to solve for the integrated coordinate. However, in cases where this iteration did converge, the implicit method (ISIA4) showed the same stability properties as SIA4.

It has been mentioned by previous authors [2, 4], that an SIA gives the exact evolution of a Hamiltonian system which is geometrically very similar to the true system. The degree of similarity is, of course, determined by the order and time step of the algorithm. Methods which are non-symplectic, however, replace the Hamiltonian system by one which is no longer Hamiltonian in nature. Consequently, after sufficiently long integration times, the numerical excitation or damping induced by such non-symplectic methods produces results which are completely uncharacteristic of the exact Hamiltonian system.

6. Summary and Conclusions

In this paper, we have generalized the method of Ruth [4] to obtain an SIA accurate to fourth order in the time step (SIA4). This algorithm has been tested using several numerical examples, including the nonlinear pendulum, the motion of a charged particle in a standing wave, and a harmonic oscillator perturbed by a plane wave. This testing has shown SIA4 to be computationally more efficient than both the classical Runge–Kutta method of order 4 (RKI4) and the implicit method given in [2]. We have also found that SIA4 is inherently more stable than RKI4 during long-time integrations.

Appendix 1

The two Runge–Kutta methods which are used to numerically integrate the vector differential equation

$$\frac{d\mathbf{x}}{dt} = \mathbf{f}(\mathbf{x}, t)$$

from the initial conditions $\mathbf{x}_0$ at time $t = t_0$ the coordinates $\mathbf{x}$ at time $t = t_0 + \delta t$ are RKI2,

$$\mathbf{x} = \mathbf{x}_0 + \mathbf{f}\left(\mathbf{x}_0 + \frac{\delta t}{2}\mathbf{f}(\mathbf{x}_0, t_0), t_0 + \frac{\delta t}{2}\right)\delta t,$$

and RKI4,

$$\mathbf{x} = \tfrac{1}{6}(\mathbf{k}_1 + 2\mathbf{k}_2 + 2\mathbf{k}_3 + \mathbf{k}_4)$$

$$\mathbf{k}_1 = \mathbf{f}(\mathbf{x}_0, t_0)\,\delta t$$

$$\mathbf{k}_2 = \mathbf{f}\left(\mathbf{x}_0 + \frac{\mathbf{k}_1}{2}, t_0 + \frac{\delta t}{2}\right)\delta t$$

$$\mathbf{k}_3 = \mathbf{f}\left(\mathbf{x}_0 + \frac{\mathbf{k}_2}{2}, t_0 + \frac{\delta t}{2}\right)\delta t$$

$$\mathbf{k}_4 = \mathbf{f}(\mathbf{x}_0 + \mathbf{k}_3, t_0 + \delta t)\,\delta t.$$

Appendix 2

The ISIA4 algorithm, shown below, for the Hamiltonian (43) is derived according to the procedure in [2]. It is accurate to fourth order in the time step. Here, (q_0, p_0) are the initial conditions at time $t = t_0$, and (q, p) are the integrated variables at time $t = t_0 + \delta t$. Note that the first equation,

$$q = q_0 + p_0\,\delta t - \frac{\delta t^2}{2}(\varepsilon \sin q \cos t) + \frac{\delta t^3}{3}(\varepsilon p_0 \cos q \cos t - \varepsilon \sin q \sin t)$$

$$+ \frac{\delta t^4}{24}[6\varepsilon p_0 \cos q \sin t + 3\varepsilon(p_0^2 + 1)\sin q \cos t - 5\varepsilon^2 \sin q \cos q \cos^2 t],$$

is implicit for q, while the second,

$$p = p_0 - \delta t(\varepsilon \sin q \cos t) + \frac{\delta t^2}{2}(\varepsilon p_0 \cos q \cos t - \varepsilon \sin q \sin t)$$

$$+ \frac{\delta t^3}{6}[2\varepsilon p_0 \cos q \sin t + \varepsilon(p_0^2 + 1)\sin q \cos t - 2\varepsilon^2 \sin q \cos q \cos^2 t]$$

$$+ \frac{\delta t^4}{24}[5\varepsilon^2 p_0 \cos^2 t(\cos^2 q - \sin^2 q) + \varepsilon(3p_0^2 + 1)\sin q \sin t$$

$$- \varepsilon p_0(p_0^2 + 3)\cos q \cos t - 10\varepsilon^2 \sin q \cos q \sin t \cos t)]$$

is explicit for p.

Acknowledgments

The authors thank R. Teshima for his expert advice on finding roots of systems of nonlinear equa-

published—a fourth-order algorithm.

REFERENCES

1. V. I. ARNOLD, *Mathematical Methods of Classical Mechanics*, 2nd ed. (Springer-Verlag, New York. 1989), p. 201.
2. P. J. CHANNELL AND C. SCOVEL, preprint, Los Alamos National Laboratory, LA-UR-88-1828, 1988 (submitted for publication).
3. T. ITOH AND K. ABE, *J. Comput. Phys.* **77**, 85 (1988).
4. R. D. RUTH, *IEEE Trans. Nucl. Sci.* **NS-30**, 2669 (1983).
5. W. E. MILNE, *Numerical Solution of Differential Equations*. 2nd ed. (Dover, New York, 1970), p. 72.
6. A. RALSTON, *A First Course in Numerical Analysis* (McGraw–Hill, New York, 1965), p. 200.
7. J. A. SANDERS AND F. VERHULST, *Averaging Methods in Nonlinear Dynamical Systems* (Springer-Verlag, New York, 1985), p. 119.
8. B. V. CHIRIKOV, *Phys. Rep.* **52**, 265 (1979).
9. G. SCHMIDT, *Comments Plasma Phys. Controlled Fusion* **7**, 87 (1982).
10. A. A. CHERNIKOV, M. YA. NATENZON, B. A. PETROVICHEV, R. Z. SAGDEEV, AND G. M. ZASLAVSKY, *Phys. Lett. A.* **122**, 39 (1986).
11. S. MURAKAMI, T. SATO, AND A. HASEGAWA, *Phys. D* **32**, 259 (1988).